Phosphorylation of NLGN4X Regulates Spinogenesis and Synaptic Function

Alexander W. Lehr,[1,2]* Thien A. Nguyen,[1,3]* (iD)Wenyan Han,[4] Eunhye Hong,[1] John D. Badger II,[1] (iD)Wei Lu,[4] and Katherine W. Roche[1]

[1]Receptor Biology Section, National Institute of Neurological Disorders and Stroke, National Institutes of Health, Bethesda, Maryland 20892, [2]Department of Neuroscience, Brown University, Providence, Rhode Island 02906, [3]Department of Pharmacology and Physiology, Georgetown University, Washington DC 20057, and [4]Synapse and Neural Circuit Section, National Institute of Neurological Disorders and Stroke, National Institutes of Health, Bethesda, Maryland 20892

Abstract

Neuroligins (NLGNs) are a family of postsynaptic adhesion molecules that bind to their presynaptic partners, neurexins, facilitating the formation and maintenance of synapses. In humans, there are five genes encoding NLGNs (*NLGN1-3*, *NLGN4X*, and *NLGN4Y*), with *NLGN1-3* having highly conserved counterparts in rodents, allowing these genes to be studied with high confidence of translational validity in mouse models. Human NLGN4X and 4Y were often assumed to serve similar functions because they share a 97% sequence homology, whereas mouse NLGN4-like is quite divergent. Many NLGN-mediated synaptic effects are modulated through post-translation modifications, which exert temporal and spatial control. In this report, we characterize a conserved phosphorylation site, serine 712, on NLGN4X and 4Y. Despite serine 712 being located in a highly conserved region between NLGN4X and 4Y, we observed kinase specificity. PKA exclusively phosphorylates NLGN4X S712, whereas Cdk5 phosphorylates S712 on both NLGN4X and 4Y. NLGN4X S712 phosphorylation regulated spine density, with phosphorylation reducing mature mushroom spines and unphosphorylated S712 increasing spines and enhancing miniature excitatory postsynaptic current frequency.

Key words: autism spectrum disorder; neuroligin; phosphorylation; sex-linked; spine morphology; spinogenesis

Significance Statement

Phosphorylation is a key regulator of synaptic function, allowing changes in protein–protein interactions and switching of protein function through the addition of a highly charged phosphate group. Neuroligins (NLGNs) are important neuronal adhesion molecules that mediate synaptic development, maintenance, and plasticity. We have now discovered analogous phosphorylation sites on the X–Y paired genes of *NLGN*, *NLGN4X* and *NLGN4Y*, which are differentially phosphorylated by PKA and Cdk5. In addition, our results reveal NLGN4X phosphorylation at this site regulates spinogenesis and spine maturation. Going forward, more research is needed to determine the role sex-linked NLGNs perform at the synapse in both physiological conditions and in neurodevelopmental disorders.

Introduction

Neuroligins (NLGNs) are postsynaptic adhesion proteins discovered through their interaction with presynaptic neurexins facilitating the close contact of the two synaptic membranes (Scheiffele et al., 2000; Sudhof, 2008; Bemben et al., 2015a; Jeong et al., 2017). In humans, NLGNs are encoded by five genes, *NLGN1-3*, *4X*, and *4Y*, each with distinct expression patterns and functions. For example, NLGN1 localizes to excitatory

synapses, whereas NLGN2 is found at inhibitory synapses, and NLGN3 is expressed at both (Chih et al., 2004; Graf et al., 2004; Chubykin et al., 2007; Poulopoloulos et al., 2009; Bemben et al., 2015b; Chanda et al., 2017). NLGNs 1 through 3 are highly conserved between humans and common model organisms like rat and mouse, allowing them to be studied with a high level of translational confidence, whereas NLGN4 is highly divergent between human and mice (Bolliger et al., 2008). *NLGN4X* and *4Y* reside in the differential region of the sex chromosomes, having arisen as an X–Y pair recently in mammalian evolution accompanying the degradation of the pseudoautosomal region of the sex chromosomes (Maxeiner et al., 2020; Nguyen et al., 2020b). NLGN4X is found at glutamatergic synapses in humans, in contrast to mouse NLGN4-like, which is found at glycinergic synapses (Hoon et al., 2011; Zhang et al., 2018). Additionally, mouse NLGN4-like is located within the pseudoautosomal region of the sex chromosome and only shares ~60% homology to human *NLGN4X/Y*.

At the synapse, protein kinases serve as an important intermediary between synaptic activity and NLGN function. For instance, surface expression of NLGN1 is modulated by Ca^{2+} calmodulin-dependent kinase II (CaMKII) phosphorylation at T739; postsynaptic density (PSD)-95 binding and endocytosis are modulated by PKA phosphorylation at S839; gephyrin binding is controlled by phosphorylation at Y782 (Bemben et al., 2014; Giannone et al., 2013; Letellier et al., 2018; Jeong et al., 2019). NLGN4X is phosphorylated by protein kinase C (PKC) at T707, and this phosphorylation event results in increased excitatory synaptic transmission (Bemben et al., 2015a). Of note, a rare variant near this phosphorylation site, R704C, was discovered in a male ASD patient, with an unaffected sister carrying the same R704C variant (Yan et al., 2005). Additional characterization revealed the ASD-associated mutant NLGN4X R704C cannot be phosphorylated by PKC at T707 and is thus unable to enhance synaptic transmission via this PKC-dependent mechanism (Bemben et al., 2015a). Taken together, phosphorylation is a dynamic mechanism to regulate and modulate NLGN function.

In this study, we identify a conserved phosphorylation site on NLGN4X and NLGN4Y, serine 712, and characterize it as a regulator of dendritic spine maturation. We show differential phosphorylation of NLGN4X and NLGN4Y at S712, depending on the kinase. Importantly, kinase specificity can be swapped through a single amino acid exchange between NLGN4X and NLGN4Y. Our characterization indicates that NLGN4X S712 is an important regulator of synaptic spine development and expands to the known role of kinases in isoform-specific NLGN regulation.

Materials and Methods

Plasmids and antibodies. Human pCAG-HA-NLGN4X (WT, S712A, S712D, or R704C)-IRES-mCherry and pCAG-NLmiRs-GFP plasmids were used for biochemical, electrophysiological, and imaging experiments. pGEX-GST-NLGN ICD constructs were made as previously described (Bemben et al., 2014). To generate the rabbit NLGN4X/4Y pS712-Ab (against residues 709–718 in NLGN4X and 4Y), we immunized the animals with synthetic phosphopeptide Ac-RRP(pS)PQRNTT-amide (New England Peptide). All immunoblotting with NLGN4X/4Y pS712-Ab begins with blocking in 5% PhosphoBLOCKER (Cell Biolabs, AKR-103) in TBS-T at room temperature, followed by 1% PhosphoBLOCKER in the primary and secondary antibody incubations. Antibodies used in the study were anti-NLGN4X (Sigma-Aldrich, sab1407790), anti-NLGN4X (Abcam, ab181251), anti-GST (Bethyl Laboratories, A190–122A), anti-HA rat (Roche, 11867423001), anti-HA rabbit (Abcam, ab9110), anti-PSD-95 (NeuroMab, 75-028), anti-actin (Applied Biological Materials, G043).

GST-fusion protein production and in vitro phosphorylation. Reagents were prepared and assays were performed and analyzed as previously described (Bemben et al., 2014).

Neuronal differentiation from iPSCs. Neural stem cells (NSCs) were differentiated from induced pluripotent stem cells (iPSCs) using the simplified doxycycline-inducible NGN2 stable hiPS cell line as described in Wang et al. (2017). hiPS cells predifferentiated into NSCs via a 3 d treatment with doxycycline were then replated. Drug treatment and cell collection were performed 3 weeks after plating, at days in vitro (DIV)21. Cells were lysed in 1% Triton X-100 buffer, and cell lysates were incubated overnight with NLGN4X/4Y

Correspondence should be addressed to Katherine W. Roche at rochek@ninds.nih.gov.

pS712-Ab and bound the subsequent day onto Protein-A beads for 1 h. The immunoprecipitated samples were washed in TBS buffer containing 150 mM NaCl, 50 mM Tris·HCl, 1 mM EDTA, as well as protease (Roche, 11836145001), and phosphatase inhibitors (Sigma-Aldrich, P5726, P0044). The sample proteins were resuspended in SDS/PAGE sample buffer, resolved by SDS/PAGE, and immunoblotted.

Neuronal cultures. Primary neuronal cultures were prepared from E18 Sprague Dawley rats and used for immunocytochemistry and phosphatase experiments. The use and care of animals used in this study followed the guidelines of the National Institutes of Health Animal Research Advisory Committee. Hippocampal neurons were plated onto glass coverslips precoated with poly-D-lysine (Sigma-Aldrich, P7280). Hippocampal neurons were cotransfected with Lipofectamine 2000 (Invitrogen, 11668-019) at DIV13 with NLmiRs and HA-NLGN4X constructs and then fixed and labeled on DIV17. Cortical neurons were plated onto poly-D-lysine–coated 10 cm tissue culture dishes at a concentration of nine million cells per dish. Primary cortical neurons were transfected with Lipofectamine 2000 at DIV5 with HA-NLGN4X WT construct, and cells were collected on DIV7, lysed in 1% Triton X-100, sonicated, and used for phosphatase treatment experiments.

Immunocytochemistry. Surface trafficking was assessed via staining surface versus intracellular HA-tagged NLGN and measuring intensities of both channels from two to three regions per secondary dendrite. To label surface proteins, live cells were incubated with primary rat HA antibody (Roche, 1186742300) at room temperature for 10 min in neurobasal media. Cells were then washed in PBS, fixed for 10 min in a 4% paraformaldehyde and 4% sucrose PBS solution, and washed again. Cells were blocked in 10% normal goat serum (NGS; Vector, S1000) and surface stained with Alexa Fluor 555-conjugated anti-rat secondary antibody (Invitrogen, A-21434) in 3% NGS. Cells were permeabilized with 0.25% Triton X-100 for 10 min, washed with PBS, and then intracellularly probed using rabbit HA antibody (Abcam, ab9110) primary and GFP (Invitrogen, A10262) to augment the signal from the GFP-fill from the NLmiRs construct and stained with Alexa Fluor 647-conjugated anti-rabbit (Invitrogen, A-21245) and Alexa Fluor 488-conjugated anti-chicken (Invitrogen, A-11039) secondary antibodies. Blinded analysis of the NLGN4X ($n = 25$), NLGN4X S712A ($n = 24$), and NLGN4X S712D ($n = 27$) conditions were averaged, and a one-way ANOVA was performed, comparing between NLGN4X WT and phosphomutant conditions.

Automated spine classification. Neurons were stained for HA, GFP, and the excitatory postsynaptic marker PSD-95 (which was not used for analysis in this study and is thus not depicted). Imaging for automated spine morphology analysis was optimized according to a previous report (Dickstein et al., 2016). Automatic spine detection and quantification were performed blinded on one to three regions of secondary dendrites per neuron using the GFP cytoplasmic fill channel with the Neurolucida 360 (MBF Bioscience) software, on NLGN4X ($n = 44$ regions), NLGN4X S712A ($n = 50$ regions), NLGN4X S712D ($n = 57$ regions), and NLGN4X R704C ($n = 44$ regions) conditions. Detection settings in Neurolucida 360 for three-dimensional reconstruction of spines were set as follows: outer range, 5 μm; minimum height, 0.3 μm; detector sensitivity, 130%; and minimum count, 10 voxels. Reconstructed spines were then manually inspected to ensure accuracy, with errant spines removed or manually reconstructed. Spines were then characterized using default setting in Neurolucida 360 (head-to-neck ratio, 1:1; length-to-head ratio, 2:5; mushroom head size, 0.35 μm; filopodium length, 3 μm).

Phosphatase treatment. Lysate from primary cortical neurons transfected with HA-NLGN4X was treated with lambda protein phosphatase. Protein concentration was measured, and 1 μg of protein was treated with 2 μl of lambda protein phosphatase (New England Biolabs, P0753S), incubated at 30°C for 30 min, resolved by SDS/PAGE, and immunoblotted.

Electrophysiological recording. The miniature excitatory postsynaptic current (mEPSC) recordings were performed in dissociated rat hippocampal primary cultures (15–17DIV). Recordings were done in artificial cerebrospinal fluid (ACSF) containing (in mM) 119 NaCl, 2.5 KCl, 26 NaHCO$_3$, 1 Na$_2$PO$_4$, 11 glucose, 2.5 CaCl$_2$, and 1.3 MgCl$_2$; 0.1 mM picrotoxin 0.1 mM and 0.5 μM TTX were added to the ACSF before recording. The intracellular solution for mEPSC recording contained the following (in mM): 135 CsMeSO$_4$, 8 NaCl, 10 HEPES, 0.3 Na3GTP, 4 MgATP, 0.3 EGTA, and 5 QX-314. The osmolality of the solutions was adjusted from 285 to 290 mOsm, and pH was buffered from 7.25 to 7.35. The mEPSCs were recorded at −70 mV, and the analysis of the mEPSCs was done semiautomatically, using the in-house software Igor Pro (WaveMetrics) developed in Roger Nicoll's laboratory at the University of California, San Francisco. All events were visually inspected to ensure they were mEPSCs during analysis, and those noncurrent traces were discarded. Series resistance was monitored and not compensated, and cells in which series resistance varied by 25% during a recording session were discarded. Synaptic responses were collected with a MultiClamp 700B amplifier (Axon Instruments), filtered at 2 kHz, and digitized at 10 kHz. All pharmacological reagents were purchased from Abcam, and other chemicals were purchased from Sigma-Aldrich.

Statistical analysis. Data analysis was conducted using ImageJ, Neurolucida360, and GraphPad Prism software. Experiments were performed blinded at least three independent times. Significant differences in phosphorylation levels were determined via conventionally utilized *t* test comparisons. For spine morphology analysis, each neuron had 1–3 secondary dendrites classified, with all individual dendrites being averaged and one-way ANOVA performed. Significance for

cumulative probability distributions in electrophysiology experiments was assessed using the Kolmogorov–Smirnov normality test with Dallal–Wilkinson–Lillie for the p value. Statistical significance is defined as $*p < 0.05$, $**p < 0.01$, $***p < 0.001$, and $****p < 0.0001$.

Results

PKA phosphorylates NLGN4X at S712

Our group has previously demonstrated that PKC phosphorylates NLGN4X at T707 (Bemben et al., 2015a; Fig. 1A). To characterize other phosphorylation sites on NLGN4X and 4Y, we used an in vitro kinase assay, with GST-fusion intracellular domains (ICDs) of NLGNs to screen for phosphorylation by several neuronal kinases (PKC, PKA, and CaMKIIα). We observed that PKC (as previously studied in Bemben et al., 2015a), PKA, and CaMKII robustly phosphorylated NLGN4X, but not 4Y (Fig. 1B). Interestingly, there is a conserved residue among all NLGN genes, which has been identified as a substrate for PKA at the analogous residue S714 in NLGN2 (Antonelli et al., 2014; Halff et al., 2022) and Cdk5 at NLGN3 S725 (Jeong et al., 2023) but is uncharacterized in NLGN4X. To study the phosphorylation of NLGN4X at the analogous S712, we developed a phosphorylation state-specific antibody using residues 709–718 as the epitope (Fig. 1C). Using an in vitro kinase assay, we validated our antibody's specificity against all NLGN ICDs as well as a phospho-dead, serine to alanine mutant of NLGN4X (S712A). We observe that our antibody robustly detects NLGN4X phosphorylated by PKA while minimally detecting the phosphonull S712A mutant, demonstrating our antibody as highly phosphospecific when compared with other phosphorylation state-specific antibodies (Fig. 1D). To confirm that our antibody recognizes phosphorylated
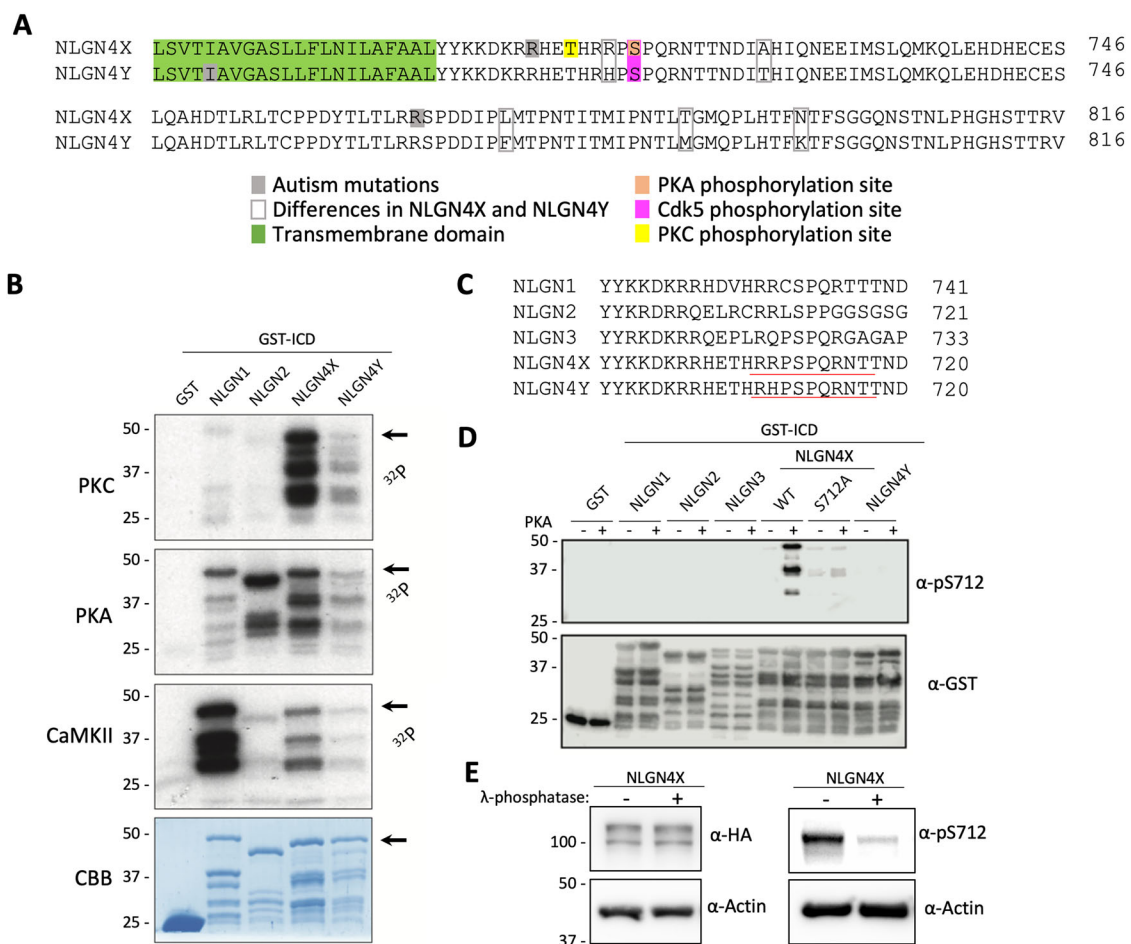

Figure 1. NLGN4X is phosphorylated by PKA at S712. **A**, Alignment of the transmembrane membrane domain and ICD of human NLGN4X and NLGN4Y. The PKC phosphorylation site, T707, is boxed in yellow; ASD mutations are boxed in gray; the transmembrane domain is boxed in blue; the PKA site on NLGN4X S712 is boxed in green; and the Cdk5 phosphorylation site on NLGN4X and NLGN4Y S712 is boxed in pink. **B**, GST-fusion proteins were incubated with [γ−^{32}P] ATP and purified PKA, PKC, and CaMKII. Phosphorylation of NLGNs was analyzed by autoradiography. CBB protein staining was used as the loading control. The arrow indicates the size of the undegraded form of GST-fused NLGN4X C-tail. **C**, Sequence alignment of NLGN1–3, 4X, and 4Y. The NLGN4X phosphorylated S712 antibody epitope is underlined in red. **D**, GST-fusion proteins of NLGN1–3, 4X (WT, S712A), or 4Y were incubated with purified PKA. PKA phosphorylation was analyzed by immunoblot probing with pS712 antibody. **E**, Lysate from transfected primary cortical neurons was treated with lambda protein phosphatase and evaluated by immunoblotting with HA-Ab or pS712-Ab. α-Actin was used as a loading control.

NLGN4X, we overexpressed NLGN4X in cortical neurons, applied phosphatase treatment to the lysate, and observed a dramatic reduction of pS712 signal when compared with basal phosphorylation levels (Fig. 1E).

To ensure that human endogenous NLGN4X is phosphorylated at S712, we utilized differentiated neurons from human iPSCs and observed phosphorylation using our phosphospecific antibody (Fig. 2A). We immunoprecipitated phosphorylated NLGN4X using our phosphospecific antibody and detected its enrichment via blotting against NLGN4X (Fig. 2B).

To determine if PKA and PKC phosphorylation were specific to their respective phosphorylation sites, we conducted additional in vitro kinase assays. Through this, we demonstrate that PKA can phosphorylate T707A, whereas PKC does not. Also, respectively, PKC can phosphorylate S712A, whereas PKA does not, demonstrating these kinases are
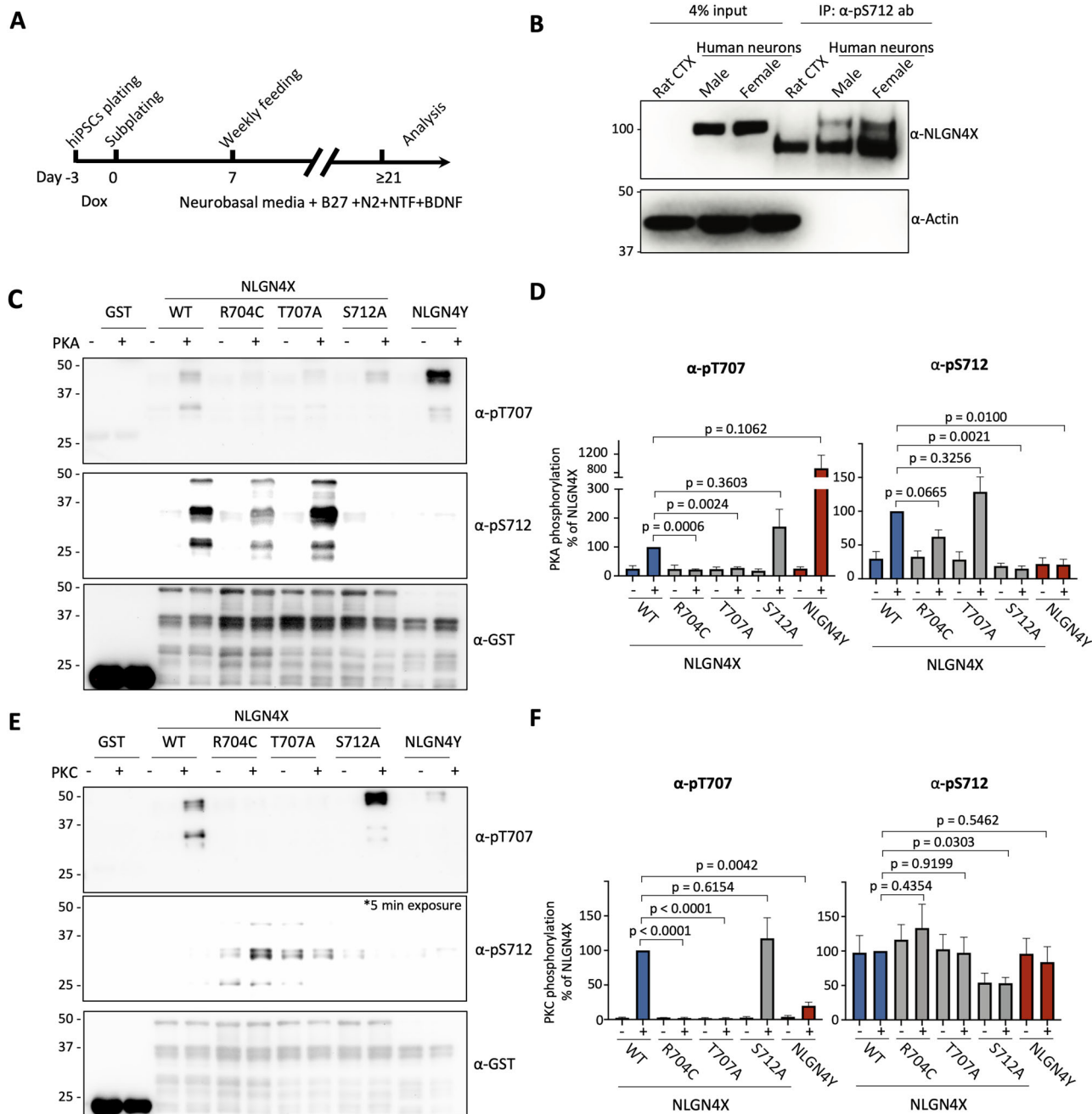

Figure 2. NLGN4X is expressed and phosphorylated at S712 in human neurons. PKA and PKC are specific to phosphorylating NLGN4X S712 and NLGN4X T707, respectively. NLGN4X R704C ASD mutation disrupts NLGN4X S712 phosphorylation. **A**, Schematic for generating induced neurons from hiPS cells. **B**, Induced neurons from hiPS cells were immunoprecipitated with NLGN4X/4Y pS712 antibody. Phosphorylation of NLGN4X was evaluated by immunoblot, probing with NLGN4X antibody. **C**, **E**, GST-fusion proteins of NLGN4X (WT, R704C, T707A, S712A) and NLGN4Y (WT) were incubated with PKC or PKA, and phosphorylation was evaluated by immunoblotting with pT707-Ab or pS712-Ab. Total protein was evaluated with GST-Ab. **D**, **F**, Phosphorylation levels (mean ± SEM) were normalized to NLGN4X. Statistical significance was tested using a t test (n = 3).

specific to their respective phosphorylation sites (Fig. 2C–F). We've previously shown that PKC phosphorylation of NLGN4X T707 is disrupted by the ASD-associated mutation R704C (Bemben et al., 2015a). In this current study, we demonstrate that the R704C mutation does not significantly disrupt the nearby PKA phosphorylation of S712 (Fig. 2C,D). It is important to note that while the R704C has been studied as an ASD-associated mutation and was recently deposited into ClinVar, this mutation does appear in many unaffected individuals in gnomAD (most of which are female).

Kinase specificity of NLGN4X and NLGN4Y is dictated by a single residue substitution

NLGN4X and 4Y have very high sequence conservation, making the differential phosphorylation surprising. We wanted to understand the molecular basis for NLGN4Y acting as a poor substrate of PKC and PKA on the conserved T707 and S712 sites as compared with NLGN4X. Examination of the NLGN4X and NLGN4Y sequences revealed one amino acid difference between the two isoforms at position 710, an arginine (R710) on NLGN4X, and a histidine (H710) on NLGN4Y. This position piqued our interest due to its intriguing location between the PKC phosphorylation site (T707) and PKA phosphorylation site (S712). We hypothesized this differential residue dictates the phosphospecificity of PKA and PKC acting exclusively on NLGN4X. Thus, we made GST-ICD NLGN4X and NLGN4Y constructs, swapping their respective 710 residues (NLGN4X R710H and NLGN4Y H710R) to determine if that would also shift the phosphospecificity of our kinases, giving PKA and PKC the ability to phosphorylate NLGN4Y and not NLGN4X. Using an in vitro kinase assay, we showed that NLGN4X R710H (containing the respective NLGN4Y histidine) was not phosphorylated by PKA and PKC. In contrast, NLGN4Y H710R can be robustly phosphorylated by both PKA and PKC (Fig. 3A–D). Together, we show that an amino acid difference between NLGN4X and NLGN4Y can account for the differential phosphorylation pattern of the two highly conserved proteins.

Cdk5 phosphorylation of NLGN4X and NLGN4Y at S712

In investigating the selective phosphorylation of NLGN4X by other kinases using in vitro kinase assays on GST-fusion ICD, we discovered that both NLGN4Y and NLGN4X were robustly phosphorylated by Cdk5 (Fig. 3E,F). We used phosphorylation of NLGN3 as a positive control for Cdk5 phosphorylation at its analogous S725 site. We thus confirmed that NLGN4X and NLGN4Y are phosphorylated at S712, unlike PKA, which only phosphorylates NLGN4X and not NLGN4Y. Thus, there is a kinase and isoform specificity to the S712 phosphorylation site.

Phosphorylation of NLGN4X at S712 decreases dendritic spine maturation

To characterize the effect of NLGN4X S712 phosphorylation, we compared the surface expression of NLGN4X (WT, S712A, or S712D) expressed in cultured rat hippocampal neurons and visualized with immunofluorescence confocal microscopy (Fig. 4A). To avoid the effects of endogenous NLGNs dimerizing with transfected NLGN4X, we cotransfected our cultured neurons with an exogenous chained microRNA against NLGNs 1, 2, and 3 (NLmiRs) as previously described (Shipman et al., 2011). Upon comparing the ratios of surface-to-intracellular NLGN4X WT with its phosphomimetic and phosphonull mutants, we did not observe any change in surface expression (Fig. 4B). Thus, we conclude that NLGN4X S712 phosphorylation does not directly affect NLGN4X surface trafficking.

We examined spine morphology to determine if NLGN4X S712A/D elicited synaptic changes despite unchanged surface expression. To quantity spine morphology, we optimized our protocol to use automatic spine detection in the neuron image analysis software, Neurolucida. Upon comparing spine densities of the various classifications of dendritic spines (mushroom, thin, stubby, or filipodia), we observed the phosphomimetic mutation of NLGN4X S712 (S712D) resulted in fewer mature mushroom spines as compared with NLGN4X WT and the phosphonull mutant (S712A; Fig. 4F). Interestingly we also observed a spinogenic effect in the phosphonull mutant, with NLGN4X S712A expressing markedly more total spines than the other conditions. This is in large part due to the significant increase in stubby spines found in the unphosphorylated condition (Fig. 4D,G). In summary, NLGN4X S712D decreases mushroom spine density compared with NLGN4X WT, consistent with fewer mature synapses. In contrast, NLGN4X S712A increases spine number, primarily through an increase in stubby spine density.

To establish the electrophysiological effects of NLGN4X phosphorylation, we recorded mEPSCs from hippocampal cultured neurons (Fig. 5A,B). These were transfected in the same manner as our immunocytochemistry experiments, cotransfecting NLGN4X, or its mutants, with NLmiRs to eliminate endogenous NLGNs, as well as a NLmiRs-only condition and a wild-type condition that was treated with Lipofectamine and no exogenous plasmids. As expected, transfection of only NLmiRs reduced both mEPSC frequencies and amplitude in primary culture hippocampal neurons. Consistent with our synaptic spine morphology data, the phosphonull NLGN4X S712A mutant increased mEPSC frequency (Fig. 5C). Both WT and phosphomimetic mutant showed no difference in mEPSC frequency or amplitude (Fig. 5C,D). Our electrophysiological studies, taken in conjunction with our spine analysis, indicate that phosphorylation of NLGN4X at S712 has a downregulatory effect on spinogenesis and spine maturation.

Discussion

In this report, we identify a novel phosphorylation site on both NLGN4X and NLGN4Y at S712. NLGN4X can be robustly phosphorylated by both PKA and Cdk5, whereas NLGN4Y is robustly phosphorylated by Cdk5 but not PKA or PKC. We identify a single amino acid difference between NLGN4X (R710) and NLGN4Y (H710), which is important for the specificity
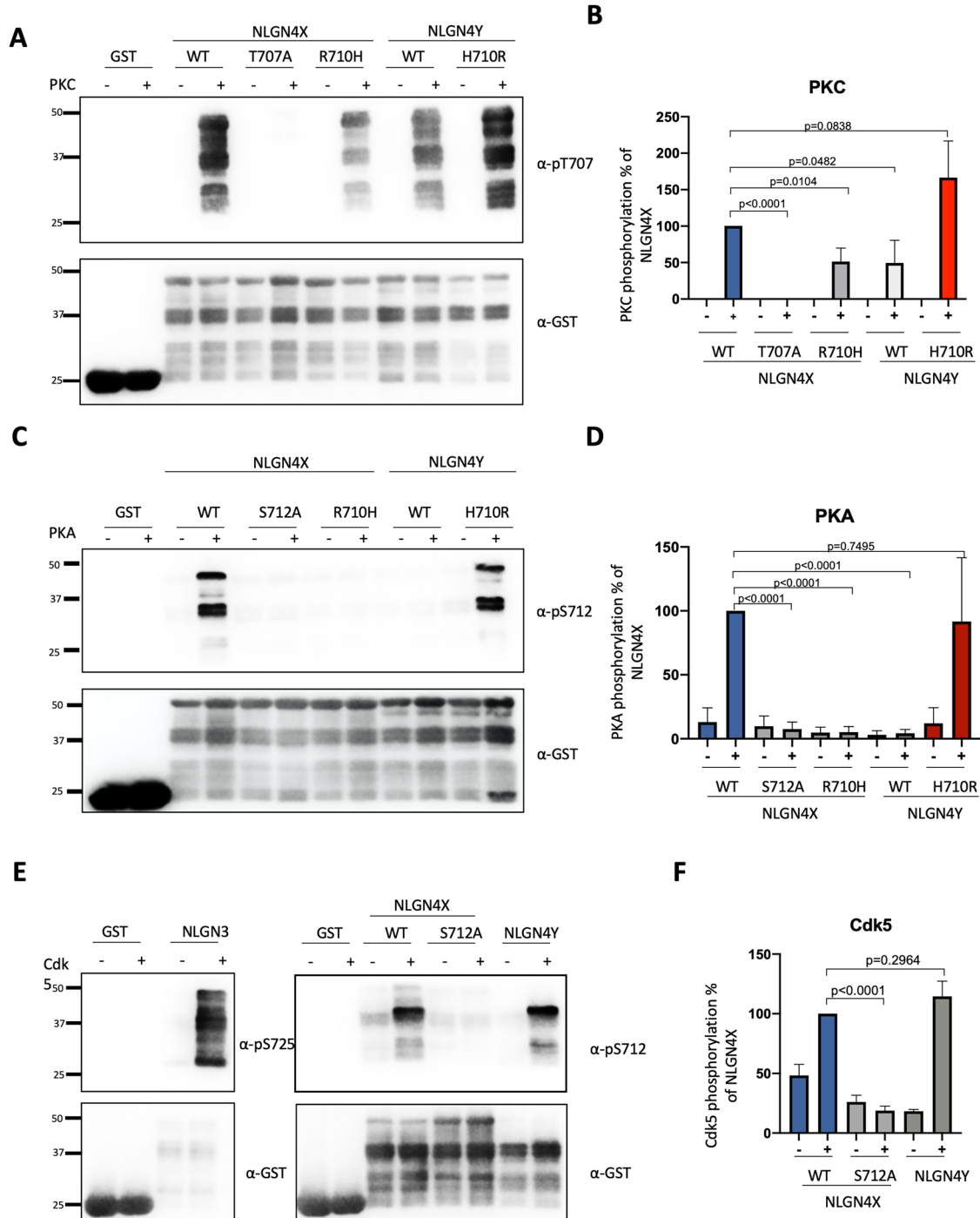
Figure 3. Serine 712 phosphorylation is conserved in NLGN4Y but shows kinase specificity. *A*, *C*, *E*, GST-fusion proteins of NLGN4X (WT, T707A, R710H, S712A) and NLGN4Y (WT, H710R) were incubated with PKC, PKA, or Cdk5, and phosphorylation was evaluated by immunoblotting with pT707-Ab or pS712-Ab. Total protein was evaluated with GST-Ab. *B*, *D*, *F*, Phosphorylation levels (mean ± SEM) were normalized to NLGN4X. Statistical significance was tested using a *t* test (*n* = 4).

of PKA phosphorylation of NLGN4X. We previously reported that NLGN4X phosphorylation via PKC in the ICD was disrupted by a familial case of ASD (Yan et al., 2005; Bemben et al., 2015a). Considering the proximity of this ASD-associated mutation (R704C) and the previously reported NLGN4X T707 PKC site, we also tested if NLGN4X S712 phosphorylation was disrupted by this ASD-associated mutation. We found PKA phosphorylation was not significantly impacted, despite the in vitro kinase assay data trending toward a reduction in phosphorylation, indicating a less dramatic but possibly biologically relevant reduction in PKA substrate affinity. Recent additions of unimpacted human variants in gnomAD call into
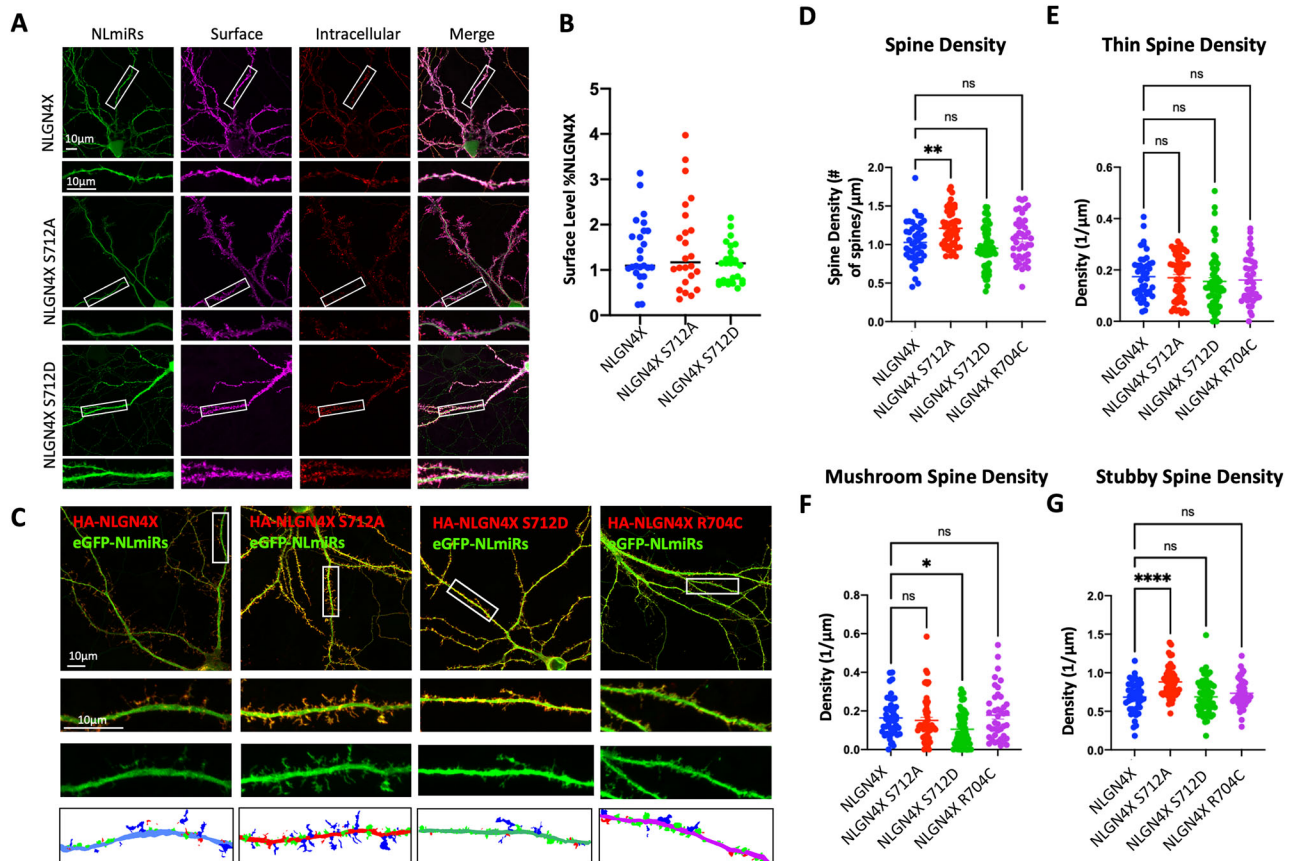
Figure 4. NLGN4X S712 phosphorylation affects spine density. **A**, Coexpression of NLmiRs with wild-type, phosphonull (S712A), and phosphomimetic (S712D) mutants in cultured hippocampal neurons. Surface and intracellular NLGN4X was labeled with HA antibody, which recognized a tag inserted downstream of the signal peptide. Scale bar, 10 μm. **B**, Mean ± SEM normalized to NLGN4X ($n = 25$), NLGN4X S712A ($p > 0.05$, $n = 24$), NLGN4X S712D ($p > 0.05$; $n = 27$). **C**, Coexpression of NLmiRs with NLGN4X WT, NLGN4X S712A, NLGN4X S712D, and NLGN4X R704C transfected into cultured hippocampal neurons. Staining was done for total HA and GFP. Reconstructed dendritic spines in the bottom panels are color coded according to the spine type (red, thin; blue, mushroom; green, stubby). **D–G**, Mean ± SEM of spine density (**D**), thin spine density (**E**), mushroom spine density (**F**), and stubby spine density (**G**) for NLGN4X ($n = 44$), NLGN4X S712A ($n = 50$), NLGN4X S712D ($n = 57$), and NLGN4X R704C ($n = 44$).

question whether this disruption is or is not pathogenic. Upon using automatic dendritic spine classification, we show that the phosphomimetic version of NLGN4X S712 decreases spine maturation. In this paper, we reveal a novel mechanism for dynamically downregulating spine maturation via NLGN4X S712 phosphorylation, which is a target for both PKA and Cdk5.

We observed an increase in immature stubby spines with NLGN4X S712A expression, which in turn increases the overall average in total spine density. We also observed a decrease in mature mushroom spines upon expression of our phosphomimetic mutant, NLGN4X S712D. The NLGN4X R704C mutation does not show the same phenotype as the NLGN4X S712A mutation, despite also disrupting NLGN4X S712 phosphorylation. This could be potentially due to NLGN4X's adjacent phosphorylation site at T707, which has been shown to increase overall spine density and EPSCs and which are disrupted by the R704C mutation (Bemben et al., 2015a). Thus, NLGN4X R704C might disrupt the spinogenic effects of NLGN4X T707 phosphorylation while possibly simultaneously promoting the spinogenic effects of NLGN4X S712 phosphorylation, hence neutralizing any observable increase in spines. We should note that our study relies on overexpression of NLGN4X in various in vitro systems, so fully understanding the physiological implications of the regulation of this phosphorylation site in vivo requires further study. Unfortunately, because NLGN4X is a human-specific gene, it is difficult to study using in vivo models.

Advances in genetic sequencing of patient populations have helped identify candidate genes with pathogenic mutations implicated in ASD, these genes often fall into functional pathways critical for synaptic function (Jamain et al., 2003; Laumonnier et al., 2004; Yan et al., 2005; Singh and Eroglu, 2013; Kenny et al., 2014; Morris-Rosendahl and Crocq, 2020; Vieira et al., 2021). ASD, defined in The American Psychiatric Association's Diagnostic and Statistical Manual, Fifth Edition (DSM-5) by deficits in social interactions accompanied by restricted and repetitive behaviors, manifests with a broad range of phenotypes with often complex genetic etiology accompanied by environmental risk factors which predilects individuals toward ASD symptoms (fifth edition; DSM-5; American Psychiatric Association, 2013). A
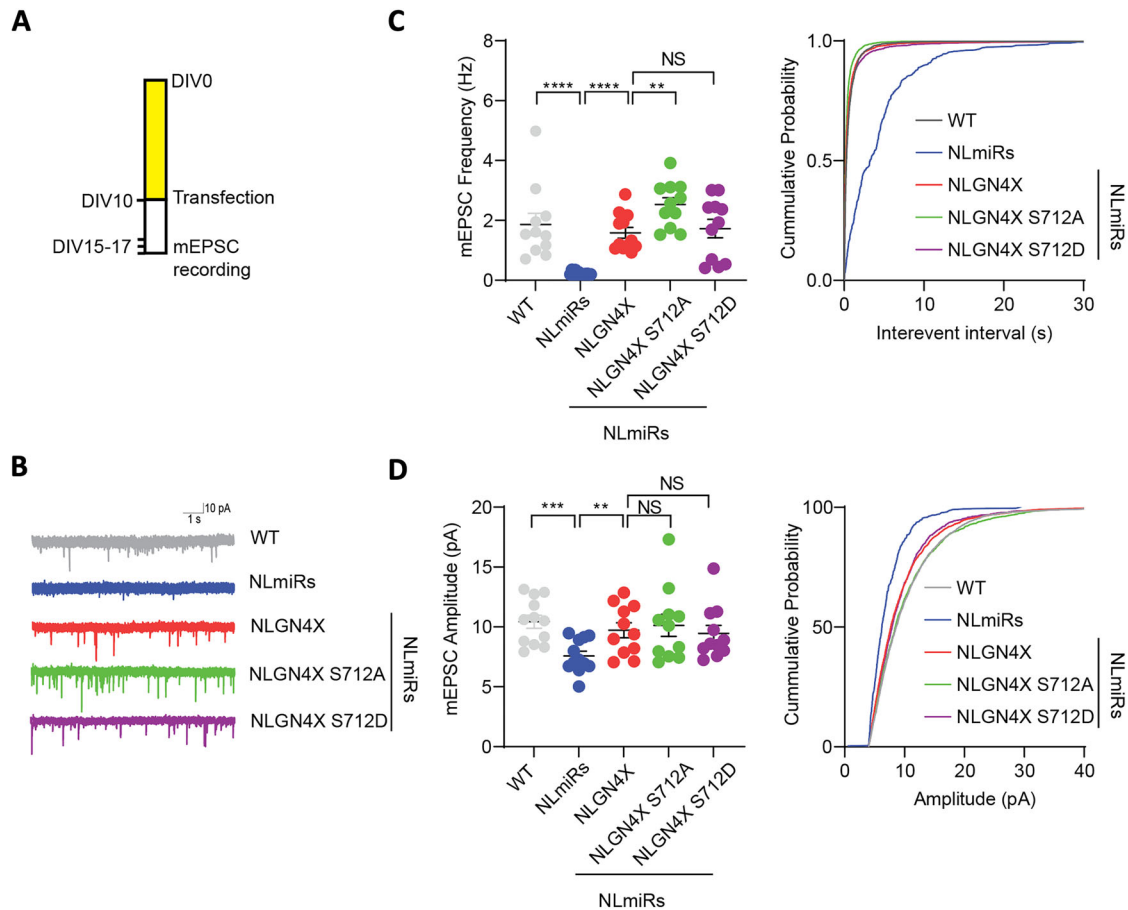
Figure 5. Phosphonull NLGN4X S712 enhances mEPSC frequency. **A**, The experimental design for transfecting and recording from primary hippocampal rat neurons, as well as representative traces of mEPSCs recorded from those cells (**B**). **C**, The mean of mEPSC frequency and cumulative probability plots of mEPSC interevent intervals and the mean of mEPSC frequency. p values were calculated using the Kolmogorov–Smirnov test with Dallal–Wilkinson–Lillie in WT ($n = 12$), NLmiRs ($n = 14$), NLGN4X WT ($n = 11$), NLGN4X S712A ($n = 11$), and NLGN4X S712D ($n = 11$) conditions. **D**, The mean of mEPSC amplitude and cumulative probability plots of mEPSC amplitude and the mean of mEPSC amplitude. p values were calculated using the Kolmogorov–Smirnov test with Dallal–Wilkinson–Lillie in WT ($n = 12$), NLmiRs ($n = 14$), NLGN4X WT ($n = 11$), NLGN4X S712A ($n = 11$), and NLGN4X S712D ($n = 11$) conditions.

family study published in 2004 linked a frameshift mutation in NLGN4X to ASD in 13 patients across four generations (Laumonnier et al., 2004). In this study, only male family members were affected with severe intellectual disability (ID) and ASD, with female carriers having no discernable phenotype. The Simons Foundation Autism Research Initiative's curated gene database scores *NLGN4X* as a Category 1 high-confidence ASD–implicated gene. To date, many of the pathogenic variants on *NLGN4X* identified are frameshift mutations, nonsense mutations, and missense mutations in the extracellular domain, with only one studied missense mutation of an arginine substituted for cysteine (R704C) located in the ICD of NLGN4X (Yan et al., 2005; Bemben et al., 2015a; Chanda et al., 2016; Marro et al., 2019; Nguyen et al., 2020a). It is important to note this variant, from a male patient, had an unimpacted sister with the same mutation, and another sister who presented with ID, thus bringing the pathogenicity of this mutation into question. Additionally, this mutation does appear in gnomAD, an aggregated database of variants from unimpacted individuals, although most of these variants appear to be female and thus could potentially be carriers. In total, there are 21 missense variants listed in ClinVar found within the ICD of NLGN4X, with varying degrees of annotation and relevance to ASD, as opposed to 85 missense variants found within the ICD appearing in gnomAD (additionally, there are 360 vs 101 missense variants found within the ECD of NLGN4X in gnomAD and ClinVar, respectively, and 13 vs 4 in the transmembrane domain).

Recent studies indicate that the NLGN4X R704C mutation is a gain-of-function mutation, enhancing AMPA receptor EPSCs and resulting in greater affinity of NLGN4X to the AMPA receptor subunit GluA1 (Marro et al., 2019). We propose a model that the NLGN4X R704C mutation, which potentially disrupts NLGN4X S712 phosphorylation thus increasing GluA1 affinity, increases the number of AMPA receptors at the PSD. Conversely, phosphorylation of NLGN4X S712 could potentially decrease NLGN4X-facilitated AMPA receptor retention at the PSD, leading to a decrease in excitatory current. This model aligns with our observations of spine morphology, with phosphomimetic NLGN4X having an increase in stubby and overall spine density. The exact mechanisms whereby NLGN4X S712 regulates AMPARs have yet to be elucidated, and further studies are needed. Thus far, there is no literature showing a direct binding of NLGNs and AMPA receptor subunits.

Also of note are studies revealing that the intracellular portion of NLGN plays a role in actin remodeling as a way of modulating synaptic plasticity (Liu et al., 2016; Paskus et al., 2019). It was shown that NLGN1's interaction with the RhoGEF Kalirin-7 is an important regulator for spine dynamics, with in vitro results demonstrating that expression of both Kalirin-7 and NLGN1 are required for NLGN1's spinogenic phenotype typically observed in primary cultured neurons (Paskus et al., 2019). With the decrease of mushroom spines in the NLGN4X S712D phosphomimetic condition, it is possible that PKA and/or Cdk5 phosphorylation of NLGN4X regulates the interaction with a downstream RhoGEF or RhoGAP, promoting actin cytoskeletal remodeling of the synapse. While thin and mushroom spines are structurally similar, mushroom spines have a larger head with a thin neck and are more persistent (Gipson and Olive, 2017; Pchitskaya and Bezprozvanny, 2020). Thus, mushroom spines are thought to be sites of long-term storage, implicating NLGN4X S712 phosphorylation as a negative modulator for long-term memory. NLGN4X could also serve as a regulator of homeostasis, acting to dampen the strengthening of synapses in response to large influxes of Ca^{2+}, or play a role in sleep, strengthening synapses when PKA levels are diminished (Hellman et al., 2010).

Specific mechanisms that direct downregulation of spine maturation upon phosphorylation of NLGN4X remain an important line of inquiry. Typically, activity-induced kinases have upregulatory effects on synaptic transmission. Our observed phenotype has an opposite effect, opening alternative avenues for the physiological importance of this phosphorylation site, and more broadly expands our understanding NLGN4X's role at the synapse.

References

American Psychiatric Association (2013) *Diagnostic and statistical manual of mental disorders*, Ed 5. Washington, DC: American Psychiatric Publishing.

Antonelli R, Pizzarelli R, Pedroni A, Fritschy JM, Del Sal G, Cherubini E, Zacchi P (2014) Pin1-dependent signaling negatively affects GABAergic transmission by modulating neuroligin2/gephyrin interaction. Nat Commun 5:5066.

Bemben MA, Shipman SL, Hirai T, Herring BE, Li Y, Badger JD 2nd, Nicoll RA, Diamond JS, Roche KW (2014) CaMKII phosphorylation of neuroligin-1 regulates excitatory synapses. Nat Neurosci 17:56–64.

Bemben MA, Nguyen QA, Wang T, Li Y, Nicoll RA, Roche KW (2015a) Autism-associated mutation inhibits protein kinase C-mediated neuroligin-4X enhancement of excitatory synapses. Proc Natl Acad Sci U S A 112:2551–2556.

Bemben MA, Shipman SL, Nicoll RA, Roche KW (2015b) The cellular and molecular landscape of neuroligins. Trends Neurosci 38: 496–505.

Bolliger MF, Pei J, Maxeiner S, Boucard AA, Grishin NV, Sudhof TC (2008) Unusually rapid evolution of neuroligin-4 in mice. Proc Natl Acad Sci U S A 105:6421–6426.

Chanda S, Aoto J, Lee SJ, Wernig M, Südhof TC (2016) Pathogenic mechanism of an autism-associated neuroligin mutation involves altered AMPA-receptor trafficking. Mol Psychiatry 21:169–177.

Chanda S, Hale WD, Zhang B, Wernig M, Südhof TC (2017) Unique versus redundant functions of neuroligin genes in shaping excitatory and inhibitory synapse properties. J Neurosci 37:6816–6836.

Chih B, Afridi SK, Clark L, Scheiffele P (2004) Disorder-associated mutations lead to functional inactivation of neuroligins. Hum Mol Genet 13:1471–1477.

Chubykin AA, Atasoy D, Etherton MR, Brose N, Kavali ET, Gison JR, Südhof TC (2007) Activity-dependent validation of excitatory versus inhibitory synapses by neuroligin-1 versus neuroligin-2. Neuron 54:919–931.

Dickstein DL, Dickstein DR, Janssen WGM, Hof PR, Glaser JR, Rodriguez A, O'Connor N, Angstman P, Tappan SJ (2016) Automatic dendritic spine quantification from confocal data with neurolucida 360. Curr Protoc Neurosci 77:1.27.1–1.27.21.

Giannone G, Mondin M, Grillo-Bosch D, Tessier B, Saint-Michel E, Czöndör K, Sainlos M, Choquet D, Thoumine O (2013) Neurexin-1β binding to neuroligin-1 triggers the preferential recruitment of PSD-95 versus gephyrin through tyrosine phosphorylation of neuroligin-1. Cell Rep 3:1996–2007.

Gipson CD, Olive MF (2017) Structural and functional plasticity of dendritic spines – root or result of behavior. Genes Brain Behav 16:101–117.

Graf ER, Zhang X, Jin SX, Linhoff MW, Craig AM (2004) Neurexins induce differentiation of GABA and glutamate postsynaptic specializations via neuroligins. Cell 119:1013–1026.

Halff EF, Hannan S, Kwanthongdee J, Lesept F, Smart TG, Kittler JT (2022) Phosphorylation of neuroligin-2 by PKA regulates its cell surface abundance and synaptic stabilization. Sci Signal 15:739.

Hellman K, Hernandez P, Park A, Abel T (2010) Genetic evidence for a role for protein kinase a in the maintenance of sleep and thalamocortical oscillations. Sleep 33:19–28.

Hoon M, et al. (2011) Neuroligin-4 is localized to glycinergic postsynapses and regulates inhibition in the retina. Proc Natl Acad Sci U S A 108:3053–3058.

Jamain S, et al. (2003) Mutations of the X-linked genes encoding neuroligins NLGN3 and NLGN4 are associated with autism. Nat Genet 34:27–29.

Jeong J, Han W, Hong E, Pandey S, Li Y, Lu W, Roche KW (2023) Regulation of NLGN3 and the synaptic Rho-GEF signaling pathway by CDK5. J Neurosci 43:7264–7275.

Jeong J, Pandey S, Li Y, Badger JD 2nd, Lu W, Roche KW (2019) PSD-95 binding dynamically regulates NLGN1 trafficking and function. Proc Natl Acad Sci U S A 116:12035–12044.

Jeong J, Paskus JD, Roche KW (2017) Posttranslational modifications of neuroligins regulate neuronal and glial signaling. Curr Opin Neurobiol 45:130–138.

Kenny EM, et al. (2014) Excess of rare novel loss-of-function variants in synaptic genes in schizophrenia and autism spectrum disorders. Mol Psychiatry 19:872–879.

Laumonnier F, et al. (2004) X-linked mental retardation and autism are associated with a mutation in the NLGN4 gene, a member of the neuroligin family. Am J Hum Genet 74:552–557.

Letellier M, Szíber Z, Chamma I, Saphy C, Papasideri I, Tessier B, Sainlos M, Czöndör K, Thoumine O (2018) A unique intracellular tyrosine in neuroligin-1 regulates AMPA receptor recruitment during synapse differentiation and potentiation. Nat Commun 9:3979.

Liu A, Zhou Z, Dang R, Zhu Y, Qi J, He G, Leung C, Pak D, Jia Z, Xie W (2016) Neuroligin 1 regulates spines and synaptic plasticity via LIMK1/cofilin-mediated actin reorganization. J Cell Biol 212:449–463.

Marro SG, et al. (2019) Neuroligin-4 regulates excitatory synaptic transmission in human neurons. Neuron 103:617–626.e6.

Maxeiner S, Benseler F, Krasteva-Christ G, Brose N, Sudhof TC (2020) Evolution of the autism-associated neuroligin-4 gene reveals broad erosion of pseudoautosomal regions in rodents. Mol Biol Evol 37:1243–1258.

Morris-Rosendahl DJ, Crocq MA (2020) Neurodevelopmental disorders—the history and future of a diagnostic concept. Dialogues Clin Neurosci 22:65–72.

Nguyen TA, et al. (2020a) A cluster of autism-associated variants on X-linked NLGN4X functionally resemble NLGN4Y. Neuron 106: 759–768.e7.

Nguyen TA, Lehr AW, Roche KW (2020b) Neuroligins and neurodevelopmental disorders: x-linked genetics. Front Synaptic Neurosci 12:33.

Paskus JD, et al. (2019) Synaptic kalirin-7 and trio interactomes reveal a GEF protein-dependent neuroligin-1 mechanism of action. Cell Rep 29:2944–2952.

Pchitskaya E, Bezprozvanny I (2020) Dendritic spines shape analysis – classification or clusterization? Perspective. Front Synaptic Neurosci 12:31.

Poulopoloulos A, et al. (2009) Neuroligin 2 drives postsynaptic assembly at perisomatic inhibitory synapses through gephyrin and collybisitin. Neuron 63:628–642.

Scheiffele P, Fan J, Choih J, Fetter R, Serafini T (2000) Neuroligin expressed in nonneuronal cells triggers presynaptic development in contacting axons. Cell 101:657–669.

Shipman SL, Schnell E, Hirai T, Chen BS, Roche KW, Nicoll RA (2011) Functional dependence of neuroligin on a new non-PDZ intra- cellular domain. Nat Neurosci 14:718–726.

Singh SK, Eroglu C (2013) Neuroligins provide molecular links between syndromic and nonsyndromic autism. Sci Signal 6:re4.

Sudhof TC (2008) Neuroligins and neurexins link synaptic function to cognitive disease. Nature 455:903–911.

Vieira MM, Jeong J, Roche KW (2021) The role of NMDA receptor and neuroligin rare variants in synaptic dysfunction underlying neurodevelopmental disorders. Curr Opin Neurobiol 69:93–104.

Wang C, et al. (2017) Scalable production of iPSC-derived human neurons to identify tau-lowering compounds by high-content screening. Stem Cell Reports 9:1221–1233.

Yan J, et al. (2005) Analysis of the neuroligin 3 and 4 genes in autism and other neuropsychiatric patients. Mol Psychiatry 10:329–332.

Zhang B, Gokce O, Hale WD, Brose N, Südhof TC (2018) Autism-associated neuroligin-4 mutation selectively impairs glycinergic synaptic transmission in mouse brainstem synapses. J Exp Med 215: 1543–1553.